NEUROSYSTEMS

Parallel pathways from motor and somatosensory cortex for controlling whisker movements in mice

EJN FEATURED ARTICLE

Varun Sreenivasan,[1,*] Kajari Karmakar,[2,3,*] Filippo M. Rijli[2,3] and Carl C. H. Petersen[1]

[1]Laboratory of Sensory Processing, Brain Mind Institute, Faculty of Life Sciences, École Polytechnique Fédérale de Lausanne (EPFL), CH-1015 Lausanne, Switzerland
[2]Friedrich Miescher Institute for Biomedical Research, Basel, Switzerland
[3]University of Basel, Basel, Switzerland

Abstract

Mice can gather tactile sensory information by actively moving their whiskers to palpate objects in their immediate surroundings. Whisker sensory perception therefore requires integration of sensory and motor information, which occurs prominently in the neocortex. The signalling pathways from the neocortex for controlling whisker movements are currently poorly understood in mice. Here, we delineate two pathways, one originating from primary whisker somatosensory cortex (wS1) and the other from whisker motor cortex (wM1), that control qualitatively distinct movements of contralateral whiskers. Optogenetic stimulation of wS1 drove retraction of contralateral whiskers while stimulation of wM1 drove rhythmic whisker protraction. To map brainstem pathways connecting these cortical areas to whisker motor neurons, we used a combination of anterograde tracing using adenoassociated virus injected into neocortex and retrograde tracing using monosynaptic rabies virus injected into whisker muscles. Our data are consistent with wS1 driving whisker retraction by exciting glutamatergic premotor neurons in the rostral spinal trigeminal interpolaris nucleus, which in turn activate the motor neurons innervating the extrinsic retractor muscle *nasolabialis*. The rhythmic whisker protraction evoked by wM1 stimulation might be driven by excitation of excitatory and inhibitory premotor neurons in the brainstem reticular formation innervating both intrinsic and extrinsic muscles. Our data therefore begin to unravel the neuronal circuits linking the neocortex to whisker motor neurons.

Introduction

Mice actively explore their environment using their mystacial whiskers, which they move back and forth at high frequencies (5–20 Hz) to scan the immediate space surrounding their snouts. When a moving whisker encounters an object the whisker bends; this exerts force at its base, driving action potentials in mechanosensitive primary sensory neurons of the trigeminal ganglion. These sensory neurons release glutamate onto postsynaptic neurons in trigeminal brainstem nuclei, from which multiple parallel sensory pathways emerge providing whisker-related tactile sensory information to other brainstem circuits, cerebellar circuits, superior colliculus and the thalamocortical system (Petersen, 2007; Diamond *et al.*, 2008; Bosman *et al.*, 2011). To generate a coherent percept of the environment, the actively acquired sensory information must be processed in the context of motor commands, e.g. to localize an object the mouse must know where the whisker was at the time of whisker–object contact (Curtis & Kleinfeld, 2009). Conversely, sensory signals affect the motor commands controlling whisker movement, e.g.

mice rapidly change whisking patterns upon active touch, presumably to enhance information flow (Mitchinson *et al.*, 2007; Crochet *et al.*, 2011). Understanding whisker tactile sensory perception therefore requires the investigation of the interactions between sensory and motor systems (Kleinfeld & Deschênes, 2011). Whereas the pathways for processing whisker sensory information have been the subject of intense investigation, much less is known about the pathways involved in whisker motor control.

The whiskers are moved by both intrinsic muscles (which are entirely located within the mystacial whisker pad) and extrinsic muscles (which attach to the mystacial pad but are anchored externally; Dörfl, 1982; Haidarliu *et al.*, 2010). Each intrinsic muscle forms a sling around an individual whisker which, upon contraction, causes the whisker to protract, pivoting around the whisker insertion point in the pad. The rhythmic contraction of intrinsic muscles is thought to be the most important process underlying exploratory whisking (Berg & Kleinfeld, 2003). On the other hand, the extrinsic muscles move the whole whisker pad and are thought to play an important role during whisker retraction (Berg & Kleinfeld, 2003). Intrinsic and extrinsic muscles are both under control of motor neurons located in the lateral facial nucleus (FN) (Klein & Rhoades, 1985; Herfst & Brecht, 2008). Classical retrograde and anterograde tracing revealed a large number of brain regions projecting to (or near to) the lateral FN (Hattox *et al.*, 2002). To specifically label premotor

neurons, genetically engineered monosynaptic rabies virus (Wickersham *et al.*, 2007) lacking glycoprotein G can be injected into muscle to infect motor neurons expressing rabies G (Stepien *et al.*, 2010). The rabies virus in the motor neurons is thus trans-complemented and can cross one synapse to infect premotor neurons. A previous study has mapped the premotor neurons for whisker muscles using rabies virus expressing fluorescent proteins (Takatoh *et al.*, 2013). Here, we extend these previous findings by analysing the overlap of cortical projections with whisker premotor neurons, revealing distinct circuits for controlling different whisker movements originating from the whisker motor cortex (wM1) and whisker somatosensory cortex (wS1) (Matyas *et al.*, 2010; Petersen, 2014).

Materials and methods

All experiments were performed in accordance with the Swiss Federal Veterinary Office, under authorization 1628 issued by the 'Service de la consommation et des affaires vétérinaires' of the Canton de Vaud.

Channelrhodopsin-2 (ChR2) virus injection

Adult (6- to 9-week-old) male and female Emx1-Cre mice [B6.Cg-Emx1$^{tm1(Cre)Krj}$/J (RRID: IMSR_JAX:005628); Cre recombinase expressed from the endogenous Emx1 locus] were deeply anesthetized with isoflurane and the body temperature was maintained at 36 °C by a heating pad. The skull was exposed and the periosteum was removed by gently scraping with a scalpel. The skull was then cleaned with Betadine. A lightweight metal head-post was fixed to the right hemisphere with cyanoacrylate glue (Henkel, Dusseldorf, Germany). A thin layer of glue was also applied over the left hemisphere to protect the skull. A chamber was made by building a wall with dental cement (Paladur, Heraeus Kulzer, Hanau, Germany) along the edge of the bone covering the left hemisphere. Dental cement was also used to reinforce the attachment of the head-post. Intrinsic signal optical imaging was carried out to map the position of the C2 barrel column in wS1. All whiskers except C2 were trimmed and the chamber over the left hemisphere was filled with warm Ringer's solution and covered with a glass coverslip. The whisker was deflected at 10 Hz for 4 s with a piezo actuator and the resulting intrinsic signal response was imaged under 630-nm illumination by a CMOS camera (Photon Focus, Lachen, Switzerland; Grinvald *et al.*, 1986). The images were processed with custom routines written in LabView (National Instruments, Austin TX, USA). To express ChR2 in excitatory neurons, we used an AAV2/5 virus expressing double-floxed humanized ChR2 (histidine 134 converted to arginine) fused to enhanced yellow-fluorescent protein (EYFP) under the control of the EF1α promoter [AAV2/5.DIO.EF1α.hChR2(H134R).EYFP, virus made by Penn Vector Core (Philadelphia, PA, USA)]. Injections were targeted either to the C2 barrel column (identified through intrinsic signal optical imaging) or to wM1 at the stereotaxic co-ordinate 1 mm anterior and 1 mm lateral to bregma. A large craniotomy (approximately 3 mm in diameter) was made over wS1 or wM1. The dura was left intact. An injection pipette (internal tip diameter approximately 20 μm) was tip-filled with the virus solution and lowered into the brain. Injections (approximately 350 nL each) were carried out at two different depths (300 and 700 μm below the pia) to infect cells in both supra- and infra-granular layers of the neocortex. The pipette was allowed to remain in the brain for 5 min before being retracted slowly over a period of 8–10 min to prevent backflow of the virus along the shaft. A cranial window was made with a circular cover slip (4 mm diameter) that was gently placed over the craniotomy. The edges were sealed with cyanoacrylate glue and dental cement (Matyas *et al.*, 2010). Three to four weeks after injection, the cranial window was assessed for YFP fluorescence using an epifluorescence microscope.

Optogenetic stimulation

For the optogenetic stimulus we used a multimode fibre-optic cable (Thorlabs, Newton, NJ, USA; numerical aperture 0.37; 400 μm) coupled to a 473 nm blue LED (Luxeon Rebel, Phillips Lumileds, San Jose, CA, USA). The outer cladding of one end of the cable was stripped and this end was glued to the LED and reinforced with epoxy and dental cement. The other end of the fibre was also stripped and mounted on a manipulator (Luigs and Neumann, Ratingen, Germany), and was lowered on to the cortical surface until the tip of the fibre-optic cable touched the cranial window. The light stimulus consisted of trains of 5-ms light flashes delivered at 50 Hz (25 pulses), or single 5-ms light flashes. The light power was approximately 10 mW.

Quantification of whisker movement

The contralateral C2 whisker was filmed at 500 Hz with a high-speed camera (Redlake, Tallahassee, FL, USA). Before applying the optogenetic stimulus, a 600-ms baseline period was recorded. All trials where the whisker was moving during this baseline period were discarded. Whisker angle was quantified using custom routines written in IgorPro (Wavemetrics, Lake Oswego, OR, USA). Power spectral density (PSD) of whisker movements upon 50-Hz blue light stimulation was calculated on a 200-ms time window before the offset of the light stimulus. The PSD was computed by squaring the amplitude spectrum, and then dividing by two times the bin size. The 5- to 20-Hz band (whisking band) power was calculated by integrating the PSD over 5–20 Hz.

Rabies virus injection in the whisker pad

The SAD-ΔG-Rabies:EGFP or SAD-ΔG-Rabies:mCherry viruses were produced in B7GG (BHK-B19G2) cells expressing glycoprotein for complementation as described previously (Wickersham *et al.*, 2010; DNA kindly provided by E. Callaway and virus kindly provided by B. Roska). Wild-type mice (male and female) at postnatal day (P)6 were anesthetized by hypothermia, by keeping them on ice for 5 min prior to injection. For retrograde tracing of the extrinsic and intrinsic motor neurons in the same animal, one of the SAD-ΔG-Rabies viruses was injected selectively into the extrinsic *nasolabialis* muscle (caudal end) and the other was injected into the intrinsic follicular muscle (C2 whisker follicle) on the right side. The volume of virus (titre – 2 × 10^6 transducing units/μL) injected into both muscles was 1.5 μL. The animals were perfused with 4% paraformaldehyde (PFA) at P8. In a different set of experiments, to confirm the cholinergic identity of labelled motor neurons, 1.5 μL of SAD-ΔG-Rabies:EGFP was injected into either the extrinsic or intrinsic muscle of ChAT-Cre × (LoxP-Stop-LoxP)-tdTomato animals [B6;129S6-ChAT$^{tm1(cre)Lowl}$/J (RRID: IMSR_JAX: 006410) × B6;129S6-Gt(ROSA)26Sor$^{tm9(CAG-tdTomato)Hze}$/J (RRID: IMSR_JAX: 007908) Jackson Laboratory, Bar Harbor, ME, USA]. For the trans-synaptic labelling experiments, SAD-ΔG-Rabies was mixed with Herpes Simplex Virus 1-Glycoprotein (HSV1-G) virus [volume ratio of HSV: Rabies; 1 : 2; 1.5 μL of mixture; Biovex (London, UK); Yonehara *et al.*, 2011], a replication-defective virus engineered to express rabies glycoprotein for complementation.

The SAD-ΔG-Rabies plus HSV1-G mix was injected at P6 into intrinsic or extrinsic muscles and the animals were killed at P11.

In some experiments, SAD-ΔG-Rabies injections in the whisker pad were coupled with anterograde tracing of cortical axons. An AAV vector encoding EGFP under the control of the synapsin promoter was used (AAV2/1.hSynapsin.EGFP.WPRE.bGH virus made by Penn Vector Core). The virus (200–500 nL) was injected stereotaxically into either wS1 (1.5 mm posterior and 2.5–3 mm lateral to bregma) or wM1 (1 mm anterior and 1 mm lateral to bregma) of P5 pups (left cortical hemisphere). SAD-ΔG-Rabies:mCherry and HSV1-G were injected unilaterally into the right whisker pad of P6 animals. The animals were killed at P11.

In situ *hybridization and immunohistochemistry*

Animals were perfused with 4% PFA. For cryostat sections, the tissue was cryoprotected in 10% sucrose (Fluka, St. Louis, MO, USA; diluted in PBS) and embedded in a solution containing 7.5% gelatin (Sigma, St. Louis, MO, USA) and 10% sucrose in PBS before being frozen at -80 °C. Coronal cryostat sections (30 μm) were cut. *In situ* hybridization against digoxigenin-labelled antisense RNA probes of *Gad67* (Lein *et al.*, 2007; Allen Brain Atlas, Gad1-RP_040324_01_F01) or *Vglut2* (Lein *et al.*, 2007; Allen Brain Atlas, Slc17a6-RP_050921_01_E03) was carried out as described in the Perkin Elmer (Waltham, MA, USA) TSA Plus fluorescence kit manual. The RNA probes were prepared by polymerase chain reaction amplification of mouse cDNA using primers for Gad67 (forward, TGT GCC AAA ACT GGT CCT; reverse, TGG CCG ATG ATT CTG GTT) and Vglut2 (forward, CCA AAT CTT ACG GTG CTA CCTC; reverse, TAG CCA TCT TTC CTG TTC CACT). The template cDNA was synthesized from total RNA extracted from embryonic day 14.5 mouse brains. The amplicons were then cloned into pCRII-TOPO vector using a TOPO TA cloning kit (Life Technologies, Carlsbad, CA, USA). The cloned plasmids were linearized by *Xho*I restriction digestion and the antisense probes were transcribed using the Sp6 RNA polymerase (Promega, Fitchburg, WI, USA). For the *in situ* hybridization, the cryostat sections were post-fixed in 4% PFA in PBS. After washing in PBS, the sections were incubated overnight at 68 °C in a probe solution (diluted in hybridization buffer, 1 : 100) in a humid chamber. Following hybridization and washing, the sections were blocked with 2% blocking reagent (Roche, Basel, Switzerland) for 1.5 h at room temperature and then incubated overnight at 4 °C with anti-digoxigenin antibody conjugated to horseradish peroxidase (1 : 100; Roche Applied Science, cat. no. 11207733910, RRID: AB_514500). After washing, the *in situ* signal was developed with TSA Plus fluorescein kit (Perkin Elmer). Following the revelation of the *in situ* signals, the sections were washed in PBS and then blocked with 5% bovine serum albumin in PBS for 1.5 h at room temperature. The sections were then incubated with rabbit anti-RFP antibody (1 : 200; Rockland Immunochemicals Inc. (Limerick, PA, USA) cat. no. 600-401-379, RRID: AB_2209751) overnight at 4 °C. Finally, they were rinsed and incubated with donkey anti-rabbit Alexa 568 (1 : 200, Life Technologies, cat. no. A10042, RRID: AB_11180183) for 2 h at room temperature.

Alignment of brainstem slices with schematic maps

Individual coronal brainstem sections were manually overlaid with the corresponding map from the Paxinos & Franklin Mouse Brain Atlas (2001). The autofluorescence of the brainstem enables the spinal trigeminal tract, the inferior cerebellar peduncle, the medial longitudinal fasciculus and the pyramidal tract to be clearly visible. Other landmarks included the midline, the fourth ventricle and the central canal. Care was taken to ensure that all the landmarks on the sections were aligned with the map. The boundaries of the brainstem nuclei were taken to be at the positions marked on the map.

Whisker pad anatomy

Animals that were injected with SAD-ΔG-Rabies into the extrinsic *nasolabialis* muscle or the intrinsic follicular muscle (C2 whisker follicle) were transcardially perfused with 4% PFA in PBS. The heads were collected and were post-fixed in 4% PFA in PBS at 4 °C overnight. They were then transferred to 20% sucrose in PBS solution for 2 days, following which they were embedded in OCT compound (Tissue-Tek; Pimos, Sakura, Japan) and allowed to freeze on dry ice. Sagittal sections of 50 μm thickness were made using a cryostat.

Statistical analysis

All data are presented as mean ± SEM. Normality of data distributions was assessed using the Anderson–Darling normality test. For normally distributed data, statistical significance was assessed with Student's *t*-test for paired or unpaired observations. For non-normally distributed data, statistical significance was assessed with Wilcoxon's rank-sum test (unpaired observations) and signed-rank test (paired observations).

Results

wS1 and wM1 drive antagonistic movements of the contralateral whisker

Our first goal was to characterize the differences in whisker movements driven by wS1 and wM1 (Haiss & Schwarz, 2005; Petersen, 2007, 2014; Matyas *et al.*, 2010). To this end, we expressed a Cre-dependent ChR2 virus in wS1 and wM1 of Emx1-Cre mice. In these mice, the expression of Cre recombinase is restricted to excitatory neurons of the neocortex (Chan *et al.*, 2001). Stimulation of wS1 with a 50-Hz light train caused a sustained retraction of the contralateral whisker whereas stimulation of wM1 with a 50-Hz light train caused a rhythmic protraction of the contralateral whisker (wS1, $-7.3 \pm 1.1°$, $n = 10$ mice; wM1, $6.0 \pm 0.9°$, $n = 8$ mice; $P = 10^{-7}$, Student's *t*-test for unpaired observations; Fig. 1A–C) (Matyas *et al.*, 2010). The latencies of wS1- and wM1-driven movements were not significantly different (wS1, 23.2 ± 6.6 ms, $n = 10$ mice; wM1, 36.5 ± 5.5 ms, $n = 8$ mice; $P = 0.1$, Wilcoxon's rank-sum test; Fig. 1C). The rhythmicities of the movements were significantly different, with wS1 driving a non-rhythmic whisker movement and wM1 driving a rhythmic whisker movement (5–20 Hz power for wS1, 5.1 ± 1.8 deg^2, $n = 10$ mice; 5–20 Hz power for wM1, 32.5 ± 6.6 deg^2, $n = 8$ mice; $P = 1.8 \times 10^{-4}$, Wilcoxon's rank-sum test; Fig. 1D).

Long stimulus trains have been shown to elicit complex movements that may involve the recruitment of other cortical areas and complex motor circuits (Graziano *et al.*, 2002; Harrison *et al.*, 2012). We therefore repeated the experiments with single brief light pulses. A single 5-ms light flash delivered to wS1 robustly evoked a small retraction of the contralateral whisker, following which the animal initiated whisking, while a 5-ms light flash delivered to wM1 caused a small protraction (wS1, $-1.4 \pm 0.4°$, $n = 6$ mice; wM1,

$1.9 \pm 0.4°$, $n = 5$ mice; $P = 10^{-4}$, Student's t-test for unpaired observations; Fig. 1E and F). The latencies of the whisker movements evoked by single 5-ms light flashes delivered to wS1 and wM1 were not significantly different (wS1, 14 ± 1 ms, $n = 6$ mice; wM1, 34.4 ± 5.7 ms, $n = 5$ mice; $P = 0.06$, Wilcoxon's rank-sum test; Fig. 1F). Thus, wS1 and wM1 drive qualitatively distinct types of whisker movements, with wS1 driving a sustained backward movement and wM1 driving a rhythmic forward movement.

Whisker motor neurons in the lateral FN

In order to understand how wS1 and wM1 cortex can drive whisker movements, we investigated the anatomical pathways involved in generating whisker motion. We began by studying the motor neurons that control forward and backward movements of the whisker. We focused our attention on the upper extrinsic muscle *nasolabialis* and the intrinsic muscles of the whisker pad. *Nasolabialis* is anchored outside the pad and extends between the vibrissa rows where it attaches superficially under the skin (Dörfl, 1982; Berg & Kleinfeld, 2003). Contraction of this muscle results in a posterior translation of the entire whisker pad, thus driving retraction of the individual whiskers. On the other hand, the intrinsic follicular muscles are located entirely within the whisker pad. Each intrinsic muscle wraps around the base of a whisker follicle to form a sling and is superficially attached to the skin surrounding the whisker that is immediately posterior. Contraction of the intrinsic muscle causes the base of the follicle to move posteriorly, thereby causing the whisker to pivot and protract (Dörfl, 1982; Berg & Kleinfeld, 2003). In order to retrogradely trace the location of the motor neurons, we injected the glycoprotein-deleted rabies virus (Rabies-ΔG; Wickersham *et al.*, 2007) encoding EGFP or mCherry into muscle of P6 mice and killed them at P8 (Fig. 2A). Analysis of the injections sites revealed that the injections were distinct and were localized to the intrinsic follicular muscle within the whisker pad and the extrinsic *nasolabialis* muscle anchored externally, respectively (Fig. 2B). The cholinergic identity of the motor neurons was confirmed by injecting Rabies-ΔG-EGFP into either the extrinsic or the intrinsic muscles of ChAT-Cre × LSL-tdTomato mice (which express the red fluorescent protein tdTomato in all cholinergic neurons; Fig. 2C and D). Injection of Rabies-ΔG-mCherry into the extrinsic muscle and Rabies-ΔG-EGFP into the intrinsic muscle (or *vice versa*) of the same animal revealed an ordered distribution of motor neurons in the FN, where the extrinsic motor neurons were always located dorsally with respect to the intrinsic motor neurons within the lateral FN (Fig. 2E and F) (Klein & Rhoades, 1985; Takatoh *et al.*, 2013). No neurons were labelled in other nuclei of the brainstem.

Intrinsic and extrinsic whisker premotor neurons in the brainstem

We were next interested in mapping the brainstem areas containing premotor neurons that synapse onto these distinct motor neuron pools. Rabies-ΔG injected into muscle is retrogradely transported to motor neurons, but the absence of the gene encoding for the glycoprotein renders it incapable of trans-synaptic spread. To allow the trans-synaptic movement of rabies, an additional retrograde virus encoding the rabies glycoprotein can be co-injected into the muscle, which will then trans-complement Rabies-ΔG in the motor neurons resulting in monosynaptic spread (Stepien *et al.*, 2010). To label the premotor neurons we injected HSV1-G, a Herpes Simplex Virus

serotype 1 vector encoding the rabies glycoprotein (Yonehara *et al.*, 2011), along with the Rabies-ΔG into extrinsic muscle (Fig. 3A), intrinsic muscle (Fig. 3A) or both muscles (Fig. 4A) of P6 mice, and killed them at P11.
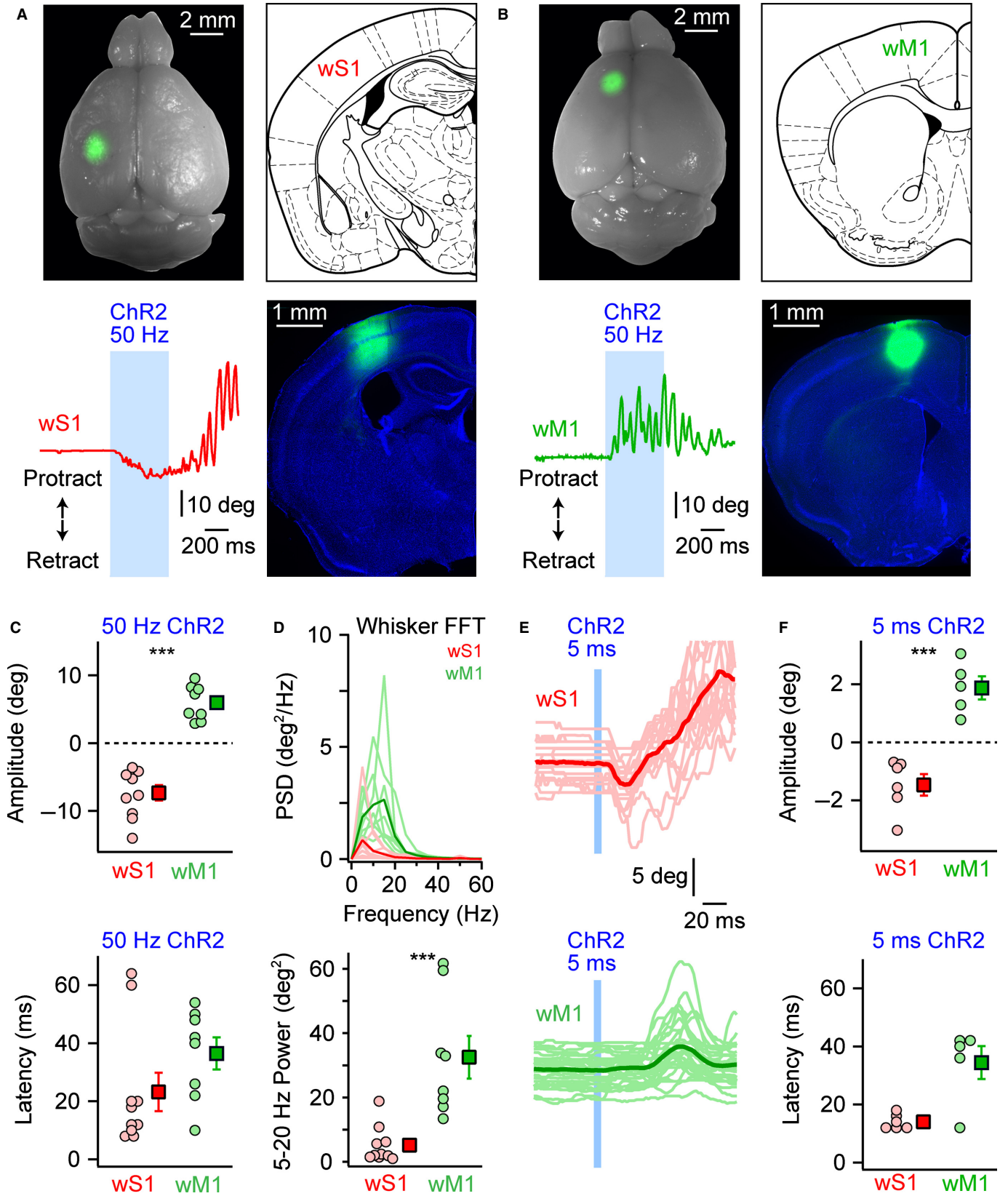
We found that the premotor neurons of these two muscles were intermingled in many brainstem areas, with very few double-labelled cells (Fig. 4). In agreement with a previous study (Takatoh *et al.*, 2013), we found intermingled premotor neurons for both extrinsic and intrinsic whisker muscles in spinal trigeminal nucleus oralis (Sp5O; Figs 3B and 4B), the vestibular nuclei (Ve; Figs 3B and 4B), the lateral para-gigantocellular nucleus (LPG), the Bötzinger/Pre-Bötzinger complexes, intermediate reticular formation (IRt; Figs 3C and 4C), gigantocellular reticular formation (GIRt), parvocellular reticular formation (PCRt; Figs 3D and 4D) and the medullary dorsal reticular formation (MdD; Fig. 3E).

We also found striking differences in the premotor distributions for intrinsic and extrinsic whisker muscles in some brainstem regions. Intrinsic premotor neurons were particularly dense along the mediodorsal to lateroventral axis of the IRt, with some cells also located more medially in GIRt. In contrast, extrinsic premotor neurons were dense in the ventrolateral aspect of spinal trigeminal nucleus rostral interpolaris (Sp5Ir), whereas there were very few intrinsic premotor neurons located in Sp5Ir. To quantify, we counted rabies-labelled premotor neurons, on the side of the brainstem ipsilateral to the injection, in coronal sections spanning Sp5O until spinal trigeminal interpolaris nucleus (Sp5Ic), and compared the total number of cells counted to the number of cells located in Sp5Ir and IRt for the extrinsic and intrinsic muscles (Fig. 3F). The fraction of extrinsic premotor neurons located in Sp5Ir was significantly higher than the fraction of intrinsic premotor neurons located in Sp5Ir (extrinsic fraction in Sp5Ir, $36 \pm 12\%$, $n = 5$ mice; intrinsic fraction in Sp5Ir, $8 \pm 3\%$, $n = 5$ mice; $P = 0.005$, Student's t-test for unpaired observations). Conversely, the fraction of intrinsic premotor neurons located in IRt was significantly higher than the fraction of extrinsic premotor neurons located in IRt (extrinsic fraction in IRt, $23 \pm 6\%$, $n = 5$ mice; intrinsic fraction in IRt, $45 \pm 12\%$, $n = 5$ mice; $P = 0.01$, Student's t-test for unpaired observations; Fig. 3F).

In summary, the premotor neurons for intrinsic and extrinsic whisker muscles were distributed in a largely intermingled manner over a large part of the brainstem. However, there were two major differences: IRt was dominated by intrinsic premotor neurons for controlling whisker protraction, and Sp5Ir was dominated by extrinsic premotor neurons for controlling whisker retraction.

Cortical innervation of the brainstem

Having identified the locations of the motor and premotor neurons for extrinsic and intrinsic whisker muscles, we next investigated the axonal innervation of the brainstem from wS1 and wM1. We injected an AAV virus encoding EGFP into either wS1 or wM1 of adult animals and studied the cortical axons in the contralateral brainstem (Fig. 5A). We found very little overlap in the brainstem regions innervated by wS1 and wM1. wS1 projected strongly to ventral Sp5O (Fig. 5B), Sp5Ir (Fig. 5C), Sp5Ic (Fig. 5D) and spinal trigeminal nucleus caudalis (Sp5C) (Fig. 5E). wM1 projected strongly to Sp5O, PCRt, GIRt, IRt, medullary ventral reticular formation (MdV) and MdD (Fig. 5B–E). wM1 also weakly innervated a dorsal portion of Sp5Ir (Fig. 5C). In addition, wM1 projected to the ventrolateral portion of the FN. To quantify, we normalized the axon intensity in the spinal trigeminal nuclei (Sp5) and the reticular formation (Rt) to the background fluores-

cence (Fig. 5F). The wS1 innervation of Sp5 was significantly stronger than the innervation of Rt (normalized axon intensity in Sp5, 2.2 ± 0.2; normalized axon intensity in Rt, 1.1 ± 0.04,

n = 3 mice; P = 0.03, Student's *t*-test for paired observations). Conversely, the wM1 innervation of Rt was significantly stronger than the innervation of Sp5 (normalized axon intensity in Sp5,

FIG. 1. Movements of the contralateral whisker driven by wS1 and wM1. (A) Widefield image of a fixed brain where ChR2-expressing virus had been injected into wS1 (top left); 50-Hz blue light stimulation of wS1 drove retraction of the contralateral whisker (bottom left). Coronal section showing the injection site localized to wS1 (right). (B) Widefield image of a fixed brain where ChR2-expressing virus had been injected into wM1 (top left); 50-Hz blue light stimulation of wM1 drove rhythmic protraction of the contralateral whisker (bottom left). Coronal section showing the injection site localized to wM1 (right). Coronal sections in panels A and B were counterstained with DAPI. (C) Quantification of whisker movement amplitudes (above) and movement latencies (below) for the 50-Hz stimulus delivered to wS1 and wM1. The amplitudes of the evoked movements were significantly different ($n = 10$ mice for wS1; $n = 8$ mice for wM1; $P = 10^{-7}$). The latencies of the evoked movements were not significantly different ($n = 10$ mice for wS1; $n = 8$ mice for wM1; $P = 0.1$). (D) PSD of the wS1- and wM1-driven whisker movements upon 50-Hz blue light stimulation (above). The PSD was calculated on a 200-ms time window before the offset of the light stimulus. The 5- to 20-Hz band (whisking band) power was significantly higher for wM1 than for wS1 (below), indicating that wM1-evoked movement was more rhythmic than wS1-evoked movement ($n = 10$ mice for wS1; $n = 8$ mice for wM1; $P = 1.8 \times 10^{-4}$). Light traces are for individual mice. Dark traces show grand average spectra. (E) A single 5-ms blue light pulse delivered to wS1 drove a small but robust retraction of the contralateral whisker (above) while a 5-ms blue light pulse delivered to wM1 drove a small but robust protraction of the contralateral whisker (below). Lighter traces indicate single trials while darker traces indicate the average for the mouse. (F) Quantification of whisker movement amplitudes (above) and movement latencies (below) for the single 5-ms stimulus delivered to wS1 and wM1. The amplitude of the evoked movement was significantly different ($n = 6$ mice for wS1, $n = 5$ mice for wM1; $P = 10^{-4}$). The latencies of the evoked movements were not significantly different ($n = 6$ mice for wS1, $n = 5$ mice for wM1; $P = 0.06$; ***$P < 0.001$).

1.4 ± 0.1; normalized axon intensity in Rt, 1.9 ± 0.3, $n = 4$ mice; $P = 0.03$, Student's t-test for paired observations; Fig. 5F). Overall, these data indicated a complementary distribution of wS1 and wM1 axons innervating the brainstem, with wS1 projecting more laterally (spinal trigeminal nuclei) and wM1 projecting more medially (brainstem reticular formation; Fig. 5F).

wS1 axons innervate extrinsic premotor neurons in Sp5Ir

Of the brainstem regions receiving dense wS1 innervation, only the Sp5Ir nucleus contained a major group of premotor neurons, mostly composed of extrinsic premotor neurons and only few intrinsic premotor neurons (Figs 3 and 4). The wS1 axons could therefore innervate extrinsic premotor Sp5Ir neurons.

However, our axonal mapping was carried out in adult mice whereas the retrograde rabies labelling of premotor neurons from muscle injections only works well in young animals. We therefore injected AAV-EGFP into wS1 and Rabies-ΔG-mCherry + HSV1-G into the contralateral extrinsic muscle of P6 mice and analysed the fixed brains at P11. We found a similar axonal innervation of the brainstem in young as compared to adult mice. Coronal sections confirmed that wS1 axons projected into the Sp5Ir region containing extrinsic premotor neurons (Fig. 6A). Imaged at high resolution with confocal microscopy (Fig. 6B), we found cortical axons in close apposition with trans-synaptically labelled extrinsic premotor neurons. We counted the number of appositions at the dendrites of these premotor neurons to be 0.07 ± 0.009 appositions/μm of dendrite
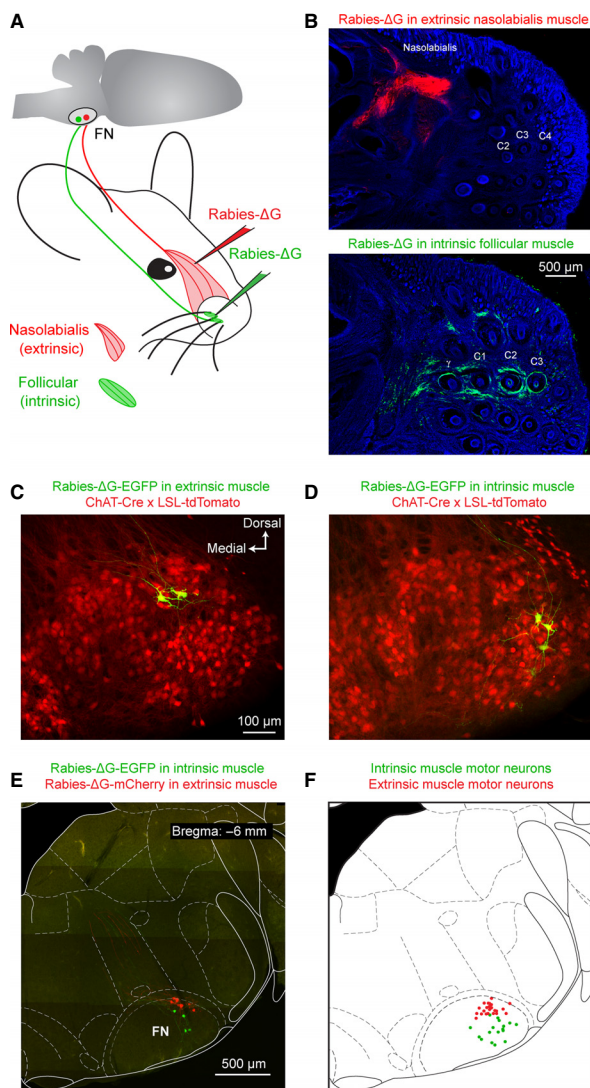
FIG. 2. The FN contains two distinct whisker motor neuron populations that drive antagonistic muscles. (A) Schematic showing the strategy used to label the motor neurons in the FN. Two different glycoprotein deleted rabies viruses (Rabies-ΔG) encoding EGFP and mCherry were injected unilaterally into the right follicular (intrinsic protractor) and right *nasolabialis* (extrinsic retractor) muscles. (B) Sagittal section of the whisker pad where Rabies-ΔG was targeted to the *nasolabialis* muscle (top) and the C2 follicular muscle (bottom). The top and bottom panels are from different animals. The pad has been counterstained with DAPI. (C) Cholinergic identity of the rabies-labelled extrinsic motor neurons was confirmed by injecting Rabies-ΔG-EGFP in the extrinsic muscle of ChAT-Cre × LSL-tdTomato animals. Double-labelled extrinsic motor neurons were present in the dorsal aspect of the lateral FN. (D) Cholinergic identity of the rabies-labelled intrinsic motor neurons was confirmed by injecting Rabies-ΔG-EGFP in the intrinsic muscle of ChAT-Cre × LSL-tdTomato animals. Double labelled intrinsic motor neurons were present in the ventral aspect of the lateral FN. (E) Coronal section through the ipsilateral brainstem at the level of the FN from an animal that received Rabies-ΔG-EGFP in the intrinsic muscle and Rabies-ΔG-mCherry in the extrinsic muscle. The red cells are the motor neurons of the extrinsic muscle while the green cells are the motor neurons of the intrinsic muscle. The coronal section is overlaid with a schematic drawing (Paxinos & Franklin, 2001). (F) Group data from seven animals that were injected with Rabies-ΔG of one colour in the extrinsic muscle and Rabies-ΔG of the other colour in the intrinsic muscle. Red circles indicate the positions of the extrinsic *nasolabialis* muscle motor neurons while green circles indicate the positions of the intrinsic follicular muscle motor neurons in the FN. The motor neurons were always located in the lateral part of the FN and the extrinsic motor neurons were located in the dorsal aspect of the lateral FN, while intrinsic motor neurons were located more ventrally.
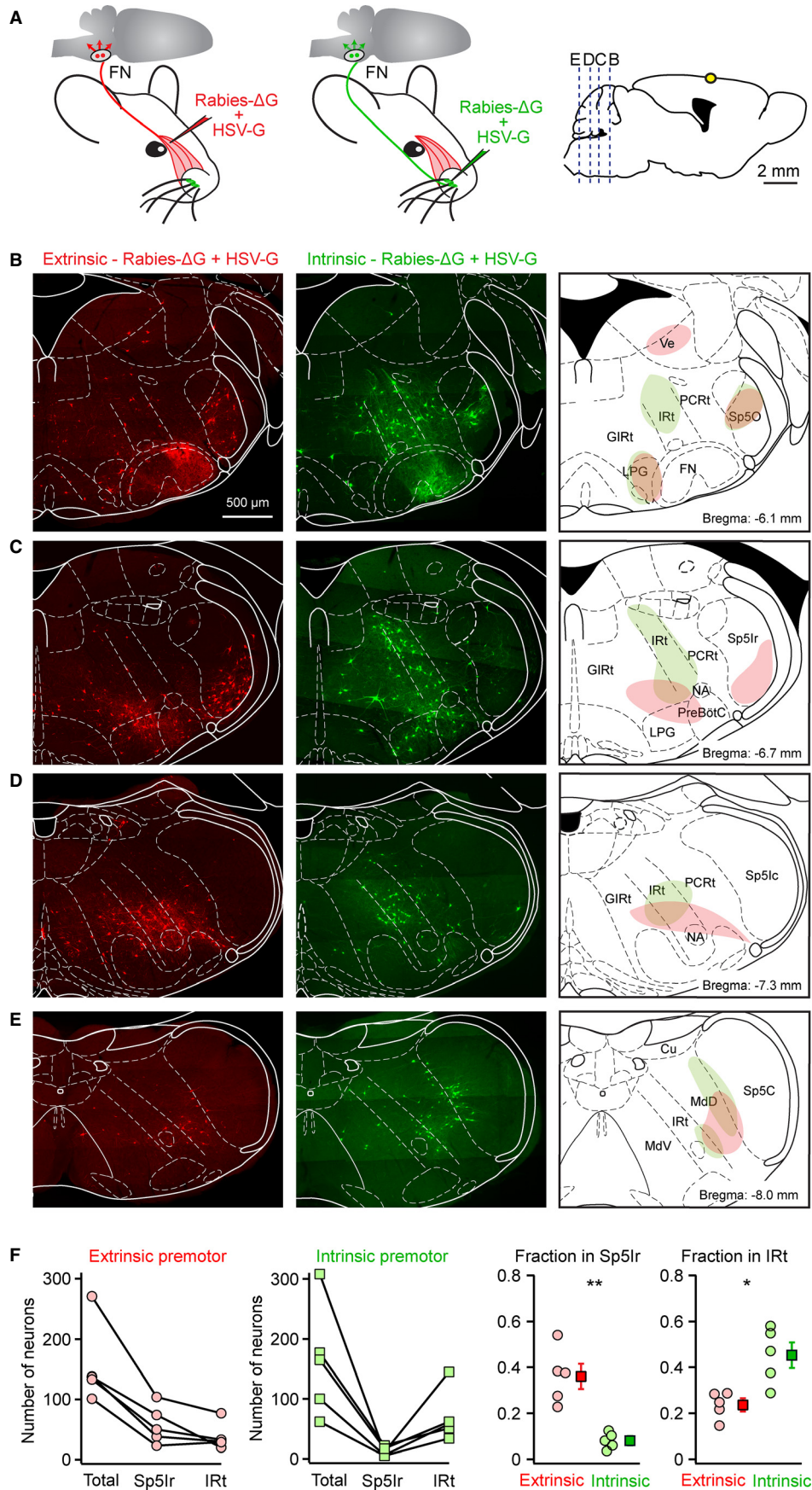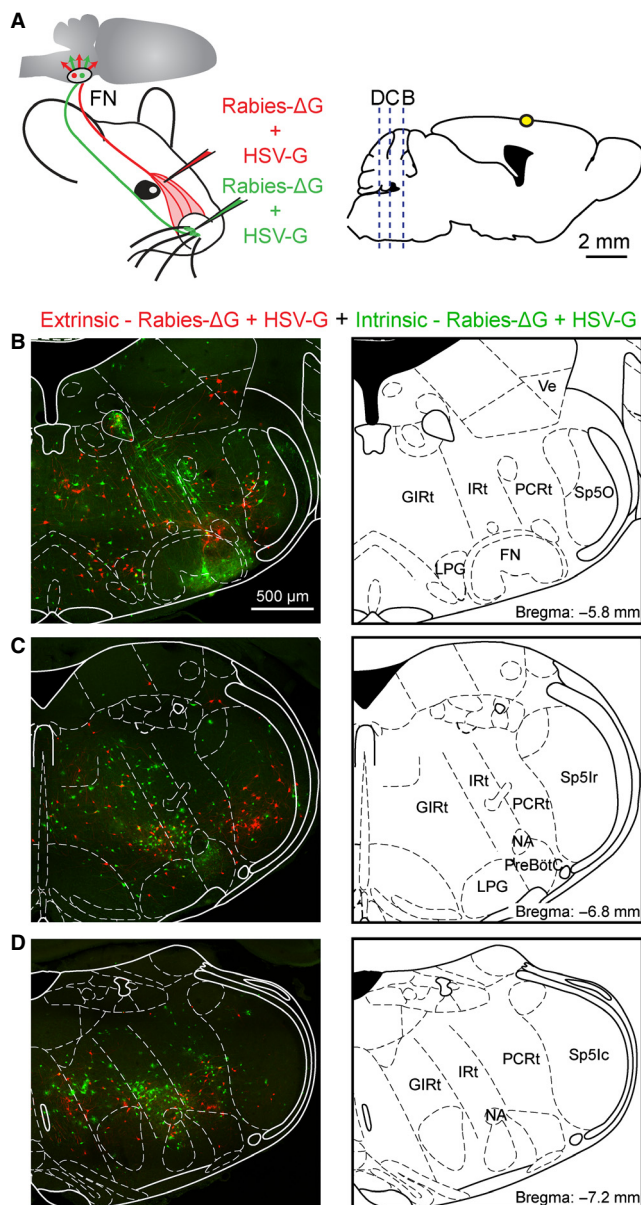
FIG. 3. Extrinsic and intrinsic premotor neurons are distributed across the ipsilateral brainstem. (A) Schematic drawing showing the strategy used to label the premotor neurons of the extrinsic and intrinsic muscles. Rabies injections were targeted to either the right extrinsic (left) or the right intrinsic (middle) muscle in individual animals. Trans-complementation was achieved by co-injecting the Herpes simplex virus serotype 1 encoding the rabies glycoprotein (HSV-G). Sagittal schematic of the brain showing the rostrocaudal positions (blue dashed lines) corresponding to the coronal sections in the subsequent panels (right). Yellow circle indicates bregma. (B) Coronal section at the level of the Sp5O. Extrinsic premotor neurons (red) were located in the Ve, the Sp5O and the LPG (left). Intrinsic premotor neurons (green) were located in the IRt, the Sp5O and the LPG (middle). (C) Coronal section at the level of the rostral part of the Sp5Ir. Extrinsic premotor neurons were located in the Sp5Ir and an area spanning the GIRt and the LPG nuclei (left). Intrinsic premotor neurons were located in the IRt (middle). The Sp5Ir contained very few intrinsic premotor neurons. (D) Coronal section at the level of the caudal part of the Sp5Ic. Extrinsic premotor neurons were located in the GIRt, IRt and ventral portion of the PCRt (*left*). Intrinsic premotor neurons were located in the IRt (middle). Some intrinsic premotor cells were also scattered in the PCRt (middle). The Sp5Ic contained very few extrinsic or intrinsic premotor cells. (E) Coronal section at the level of the Sp5C. Extrinsic (left) and intrinsic (middle) premotor neurons were located in the MdD and the IRt. The Sp5C did not contain either extrinsic or intrinsic premotor cells. The coronal images in panels B–E are overlaid with the corresponding schematic drawings (Paxinos & Franklin, 2001). Simplified schematic maps of premotor neurons are summarized based on consistent results from five mice for each injection (right). Red regions indicate areas with many extrinsic premotor neurons, green regions show high density of intrinsic premotor neurons and the brown regions indicate areas occupied by both extrinsic and intrinsic premotor neurons. (F) Quantification of number of labelled extrinsic premotor neurons ($n = 5$ mice, far left) and intrinsic premotor neurons ($n = 5$ mice, middle left). In Sp5Ir, the fraction of extrinsic premotor neurons was significantly higher than the fraction of intrinsic premotor neurons (middle right). In the IRt, the fraction of intrinsic premotor neurons was significantly higher than the fraction of extrinsic premotor neurons (far right); *$P < 0.05$; **$P < 0.01$.

(11 dendrites from three premotor cells in two mice). These data indicate that wS1 and Sp5Ir extrinsic premotor neurons are likely to be synaptically connected.

FIG. 4. Double-labelling of extrinsic and intrinsic premotor neurons in the ipsilateral brainstem. (A) Schematic showing the strategy used to label premotor neurons of the extrinsic and intrinsic muscles in the same animal. Two different Rabies-ΔG viruses encoding EGFP and mCherry were injected unilaterally on the right side of the same mouse into the intrinsic muscle and extrinsic muscle respectively (left). Trans-complementation was achieved by co-injecting the Herpes simplex virus serotype 1 encoding the rabies glycoprotein (HSV-G). Sagittal schematic of the brain showing the rostrocaudal positions (blue dashed lines) corresponding to the coronal sections in the subsequent panels (right). Yellow circle indicates bregma. (B) Coronal section through the FN and Sp5O in a mouse that received Rabies-ΔG-mCherry + HSV-G in the extrinsic muscle and Rabies-ΔG-EGFP + HSV-G in the intrinsic muscle. Note the intermingled cell distributions in Sp5O and LPG. (C) Coronal section through Sp5Ir of the same mouse. Note the presence of red extrinsic premotor neurons and sparsity of green intrinsic premotor neurons in Sp5Ir. The IRt has a large number of green intrinsic premotor neurons. (D) Coronal section through Sp5Ic of the same mouse. The Sp5Ic contains neither extrinsic nor intrinsic premotor neurons. Also note the presence of green intrinsic premotor neurons in the IRt region near the NA. The coronal images in panels B–D are overlaid with the corresponding schematic drawings (right) (Paxinos & Franklin, 2001). The premotor neuron distributions observed in double-labelled mice were consistent across four mice.

We next investigated the neurotransmitter phenotype of Sp5Ir premotor neurons by *in situ* hybridization for *GAD67* and *Vglut2*. The analysis revealed that the large extrinsic premotor neurons labelled in Sp5Ir were glutamatergic (Fig. 6C). A few of the smaller extrinsic premotor neurons were GABAergic (Fig. 6C). As the large glutamatergic extrinsic premotor neurons located in Sp5Ir receive excitatory input from pyramidal neurons of the contralateral wS1, we reason that wS1→Sp5Ir (extrinsic premotor)→FN (extrinsic motor) constitutes a motor circuit in which stimulation of wS1 could drive retraction of the contralateral whisker (Fig. 6D).

wM1 axons innervate the FN and IRt

We were next interested in the motor circuits downstream of wM1. A previous study reported the presence of monosynaptic connections from wM1 onto motor neurons in the FN of the rat (Grinevich *et al.*, 2005). Accordingly, we observed AAV-EGFP-labelled wM1 axons projecting to the ventrolateral aspect of the contralateral FN labelled in ChAT-Cre × LSL-td-Tomato mice (Fig. 7A). Furthermore, trans-synaptic rabies tracing from the intrinsic muscle also identified intrinsic premotor neurons in frontal and wM1 cortex (Fig. 7B). In contrast, very few cortical neurons were labelled when trans-synaptic rabies virus was injected into extrinsic muscle. Thus,

A   AAV-EGFP in wS1   AAV-EGFP in wM1

Axons to brainstem   Axons to brainstem

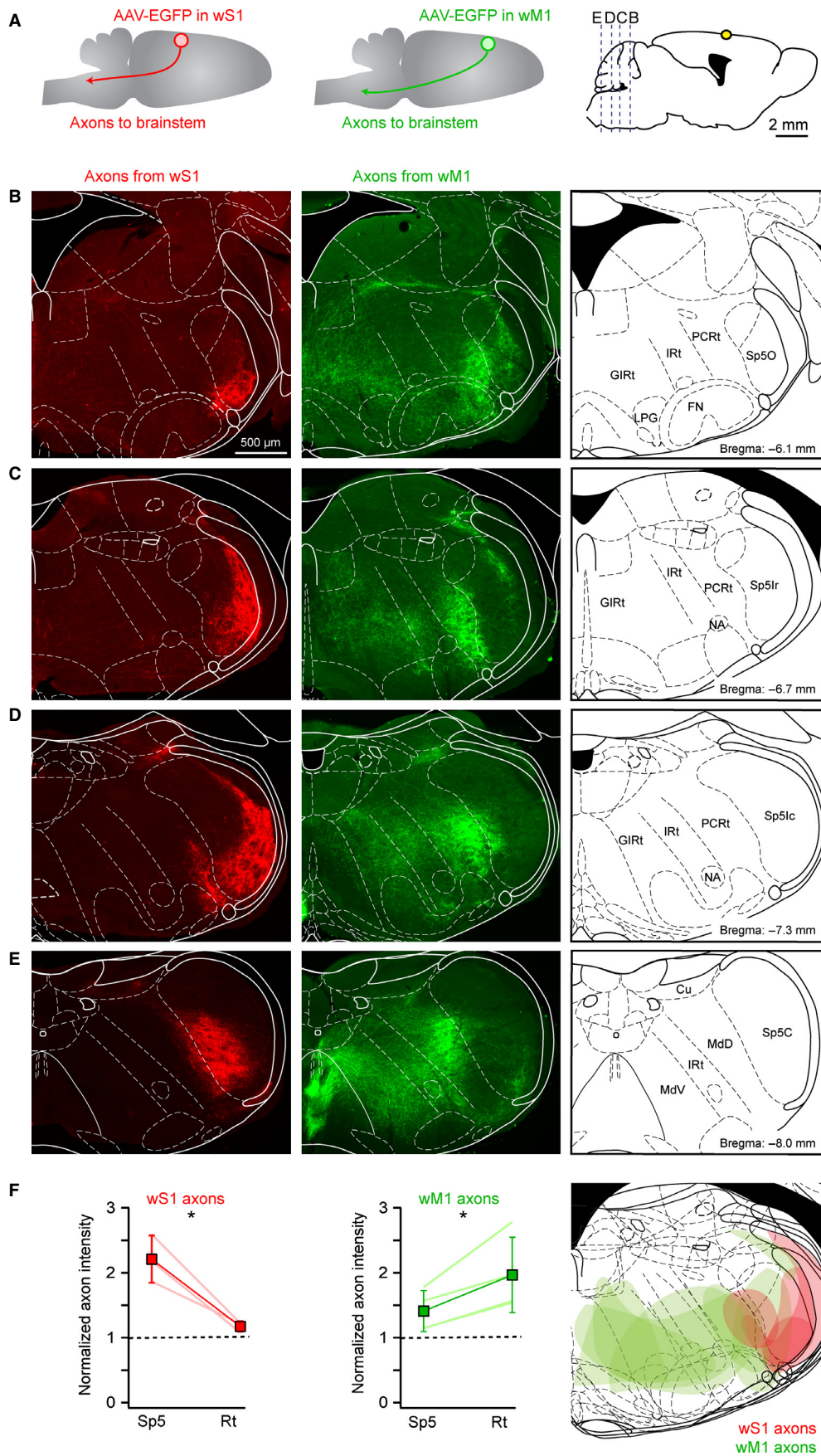**B**   Axons from wS1   Axons from wM1

FIG. 5. Cortical axons in the contralateral brainstem. (A) AAV virus encoding EGFP was injected into either wS1 (left) or wM1 (middle) of adult mice. Sagittal schematic of the brain showing the rostrocaudal positions (blue dashed lines) corresponding to the coronal sections in the subsequent panels (right). Yellow circle indicates bregma. (B) Coronal sections at the level of Sp5O. At this level, wS1 axons densely innervated the ventral Sp5O (left) while wM1 axons innervated GIRt, the lateral FN and the PCRt (middle). (C) Coronal sections at the level of Sp5Ir. At this level, wS1 axons densely innervated the Sp5Ir (left) while wM1 axons densely innervated the PCRt and diffusely innervated the IRt and GIRt (middle). (D) Coronal sections at the level of Sp5Ic. At this coronal level, wS1 axons densely innervated the Sp5Ic (left) while wM1 axons densely innervated the PCRt and diffusely innervated the IRt and GIRt (middle). (E) Coronal sections at the level of Sp5C. At this coronal level, wS1 axons densely innervated the Sp5C (left) while wM1 axons broadly innervated the MdD, IRt and MdV nuclei (middle). The coronal images in panels B–E are overlaid with corresponding schematic drawings (right) (Paxinos & Franklin, 2001). (F) Quantification of axon intensity in the spinal trigeminal nuclei (Sp5) and the reticular formation (Rt) in animals that received the virus injection in wS1 (left) and wM1 (middle). The axon intensity was normalized to the background fluorescence (dashed line at 1). Sp5 received significantly stronger input than the Rt from wS1, while the Rt received significantly stronger input than Sp5 from wM1. Schematic drawing showing the distribution of axons from wS1 and wM1 (right). Coronal maps were aligned to the images and a contour was drawn around the axon termination sites. The maps were then superimposed. Note that wS1 largely innervates the spinal trigeminal nuclei while wM1 largely innervates the reticular formation. Some overlap is evident in Sp5O, the ventral part of PCRt and the MdD; *$P < 0.05$.

wM1 might contribute to controlling whisker movements by directly synapsing onto the motor neurons innervating intrinsic muscles.

A major innervation site of the wM1 axons in the brainstem was the PCRt (Fig. 5D). However, in our rabies tracing experiments we did not consistently find premotor cells localized in PCRt and, in the cases in which we did, they were few in number and did not display any specific distribution or clustering. Furthermore, lesioning

the PCRt has little effect upon whisker movements (Moore *et al.*, 2013).

Next we investigated the wM1 projections in the IRt. It has been suggested that a whisking central pattern generator in the brainstem is localized in the ventral part of the IRt, lying medial to the nucleus ambiguus (NA) (Moore *et al.*, 2013). As the NA contains cholinergic neurons, it is easily distinguishable in the ChAT-Cre × LSL-tdTomato animals (Fig. 7C). We found that wM1 innervated the region of the IRt near to the NA (Fig. 7C, middle). This region was a major hotspot of intrinsic premotor neurons (Fig. 7C, right). To investigate the potential overlap of the wM1 axons with these premotor neurons, we injected AAV-EGFP into wM1 and Rabies-ΔG-mCherry + HSV1-G into the contralateral intrinsic muscle of P6 mice and killed them at P11. Coronal sections showed that, in the IRt, the wM1 axons came into close apposition with the trans-synaptically labelled intrinsic premotor neurons (Fig. 7D). We counted the number of appositions at the dendrites of these premotor neurons to be 0.06 ± 0.008 appositions/μm of dendrite (11 dendrites from three premotor cells in two mice). The rabies-labelled population of premotor neurons in the IRt contained both GAD67^{+} inhibitory neurons and Vglut2^{+} excitatory neurons (Fig. 7E). wM1 might thus innervate both excitatory and inhibitory intrinsic premotor neurons. In addition, the same brainstem region also harbours extrinsic premotor neurons. wM1 innervation of IRt (and surrounding brainstem reticular regions) might thus drive rhythmic whisker protraction through a complex network of inhibitory and excitatory premotor neurons for both intrinsic and extrinsic muscles, which might constitute an oscillatory central pattern generator (Fig. 7F) (Moore *et al.*, 2013).
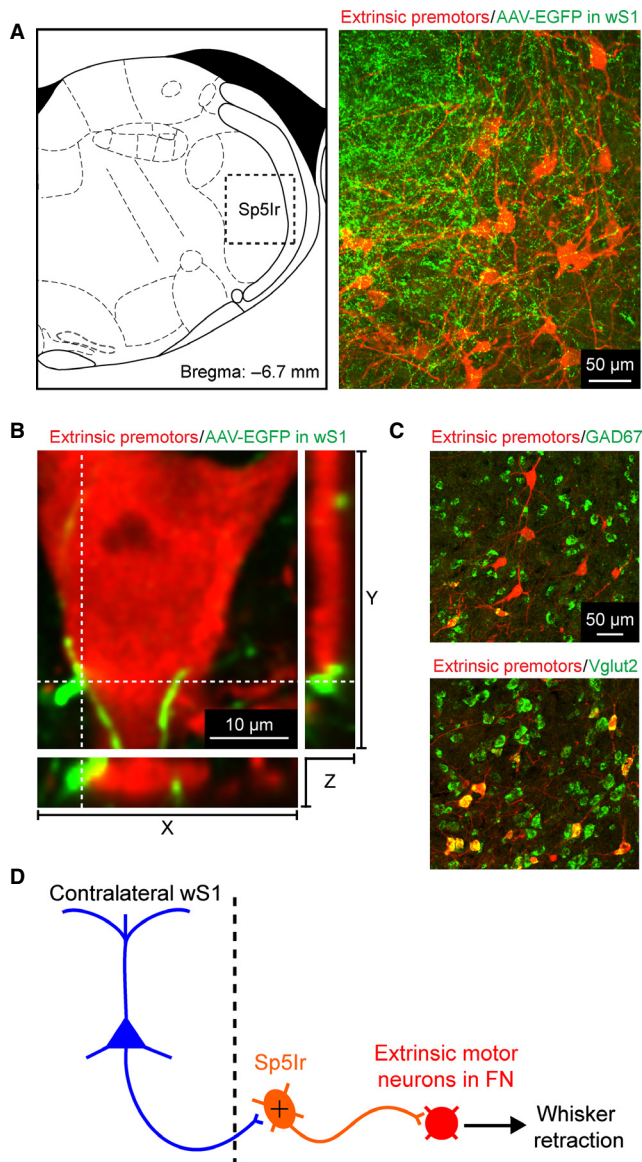
Discussion

To further our understanding of the cortical circuits involved in whisker motor control, we characterized the whisker movements dri-

FIG. 6. Extrinsic premotor neurons in Sp5Ir receive input from contralateral wS1. (A) Coronal schematic drawing at the level of the Sp5Ir (left) (Paxinos & Franklin, 2001). Blue dotted box indicates the area shown in the right panel. AAV virus encoding EGFP was injected into wS1 in the left hemisphere, to label the cortical axons in the brainstem. In the same animal, Rabies-ΔG-mCherry + HSV-G was injected into the right extrinsic muscle to label the premotor neurons. In the contralateral Sp5Ir, the wS1 axons densely innervated the region containing extrinsic premotor neurons (right). (B) Orthogonal projections in *xy*, *xz* and *yz* planes show close apposition between the cortical axon (green) and the premotor neuron (red) located in Sp5Ir. (C) The neurotransmitter phenotypes of the labelled neurons in Sp5Ir were determined with fluorescent *in situ* hybridization. The large cells in Sp5Ir were negative for GAD67 (top) but were positive for Vglut2 (bottom). These cells were excitatory. A few smaller cells in Sp5Ir were positive for GAD67 (top) and negative for Vglut2 (bottom). These cells were inhibitory. (D) Schematic showing a possible motor circuit by which wS1 might drive whisker retraction.

A ChAT-Cre x LSL-tdTomato — AAV-EGFP in wM1

Bregma: −5.8 mm

FN

500 μm

20 μm

B wM1 — FN — Rabies-ΔG + HSV-G — Intrinsic muscle

Bregma: 1.4 mm — wM1

DAPI/Intrinsic premotors

20 μm

200 μm

C IRt NA — Bregma: −7.0 mm

ChAT/AAV-EGFP in wM1

NA

100 μm

ChAT/Intrinsic premotors

NA

100 μm

D Intrinsic premotors/wM1 axon

50 μm

Intrinsic premotors/wM1 axon

Y

Z

X

10 μm

E Int. premotors/GAD67

50 μm

Int. premotors/Vglut2

F Contralateral wM1

IRt

FN
Intrinsic muscle
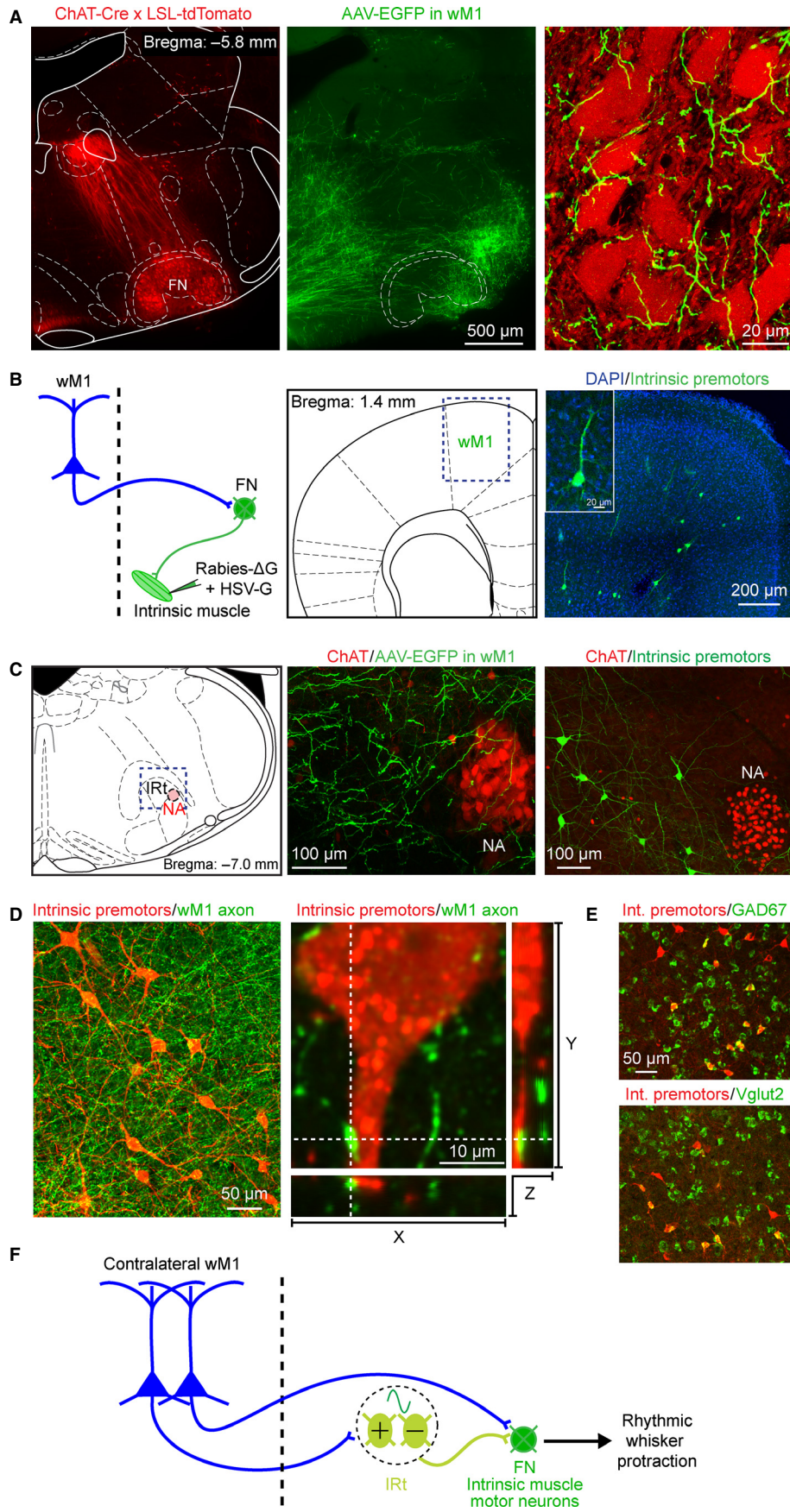motor neurons

Rhythmic
whisker
protraction

FIG. 7. Intrinsic motor neurons in FN and premotor neurons in IRt receive input from contralateral wM1. (A) Coronal section through the FN of a ChAT-Cre × LSL-tdTomato mouse. The corresponding schematic drawing is overlaid (left). To investigate the potential innervation of FN by wM1, an AAV virus encoding EGFP was injected into wM1 of ChAT-Cre × LSL-tdTomato mice. The wM1 axons (green) project to the contralateral FN, predominantly in the ventral aspect (middle). The images in the left and middle panels are of the same slice. High-resolution confocal image of the ventrolateral FN, showing the EGFP-expressing wM1 axons in close apposition with the tdTomato-expressing motor neurons (right). (B) If wM1 neurons synapse directly onto the motor neurons located in the ventrolateral FN, then Rabies-ΔG + HSV-G injections in the intrinsic muscle should label premotor neurons in wM1 (left). Coronal schematic drawing (Paxinos & Franklin, 2001) at the level of wM1 (middle) with a blue dotted box indicating the area of wM1 shown in the right panel. Intrinsic premotor neurons were present in wM1 with labelled neurons located in layers 5 and 6 (right). The inset shows a labelled cell in wM1 at higher resolution. (C) Coronal schematic drawing (Paxinos & Franklin, 2001) at the level of the NA (left). Blue box indicates the area of the IRt shown in the middle and right panels. The wM1 axons projected to the IRt region near to the NA (middle). This region was also a major hotspot of intrinsic premotor neurons (right). (D) AAV virus encoding EGFP was injected into wM1 of the left hemisphere to label the cortical axons in the brainstem. In the same mouse, Rabies-ΔG-mCherry + HSV-G was injected into the right intrinsic muscle to label the premotor neurons. In the right IRt, the wM1 axons innervated the intrinsic premotor neurons near to the NA (left). Orthogonal projections in *xy*, *xz* and *yz* planes show close apposition between the cortical axon (green) and the premotor neuron (red) located in the IRt (right). (E) The neurotransmitter phenotypes of the labelled neurons in the IRt were determined with fluorescent *in situ* hybridization. The population of labelled intrinsic premotor neurons in the IRt contained GAD67-positive inhibitory neurons (top) as well as Vglut2-positive excitatory neurons (bottom). (F) Schematic drawing of a possible circuit by which wM1 might drive whisker movement. The '+' indicates excitatory intrinsic premotor neurons and '−' indicates inhibitory intrinsic premotor neurons in the IRt. Together, these might constitute an oscillator that drives rhythmic whisker protraction.

ven by wS1 and wM1. Optogenetic stimulation of wS1 evoked whisker retraction while optogenetic stimulation of wM1 evoked whisker protraction that was rhythmic (Fig. 1). We used modified rabies virus to map whisker motor (Fig. 2) and premotor (Figs 3 and 4) neurons, and we investigated the axonal projections from wS1 and wM1 to the brainstem using AAV virus (Fig. 5). We examined the regions with the most prominent overlap between cortical axons and premotor neurons finding that wS1 axons strongly overlap with extrinsic premotor neurons located in the Sp5Ir (Fig. 6) and that wM1 axons overlap with intrinsic premotor neurons in IRt (Fig. 7). In addition we found that wM1 innervates the intrinsic motor neurons in FN (Fig. 7). Together our results suggest that wS1 and wM1 control distinct whisker movements through two parallel motor pathways.

Distinct whisker premotor neuron subpopulations for intrinsic and extrinsic muscles

Rabies virus has been used extensively as a retrograde trans-synaptic tracer to map motor circuits in the mammalian brain. Pioneering work used replicating rabies virus to trace motor control circuits across multiple synapses (Ugolini, 1995; Rathelot & Strick, 2006). Monosynaptic inputs can be traced using genetically modified rabies virus (Wickersham *et al.*, 2007) and this approach has recently been applied to map premotor neurons (Stepien *et al.*, 2010; Takatoh *et al.*, 2013; Esposito *et al.*, 2014). Our results investigating the premotor circuits for whisker motor control are in good agreement with a previous study by Takatoh *et al.* (2013). The extrinsic muscle *nasolabialis*, which is involved in retracting the whisker, is innervated by motor neurons located in a more dorsal part of the lateral FN than the motor neurons innervating the intrinsic follicular muscles involved in protracting the whisker (Fig. 2). The premotor neurons providing input to these distinct motor neuron pools are also largely segregated, with very few double-labelled premotor neurons (Fig. 4). In some regions of the brainstem (such as Sp5O, LPG and caudal IRt) the premotor neurons for intrinsic and extrinsic muscle are intermingled (Figs 3 and 4). However, in other parts of the brainstem there are large differences in the density of premotor neurons innervating intrinsic and extrinsic muscles. The most prominent differences are in Sp5Ir, which is strongly dominated by extrinsic premotor neurons with very few intrinsic premotor neurons, and IRt, which is dominated by intrinsic premotor neurons (Figs 3 and 4). The rhythmic back-and-forth movements of the whiskers during exploration are largely driven by the intrinsic muscles. The prominence of intrinsic premotor neurons in IRt is consistent with an important role in whisking for this brainstem

region which, it has been suggested, forms the central pattern generator (Moore *et al.*, 2013).

The mechanisms of trans-synaptic spread of rabies virus is unknown and, recently, the specificity of retrograde vs. anterograde transport has been called into question (Zampieri *et al.*, 2014). In our experiments, we do not find evidence for anterograde trans-synaptic spread. If the rabies virus was spreading in an anterograde direction then one would expect to see trans-synaptic labelling of neurons in the sensory trigeminal nuclei via infection of the trigeminal primary sensory neurons. However, we did not find any rabies-labelled neurons in the principal trigeminal (Pr5) nucleus or in the caudal sector of Sp5Ic. Thus, under our experimental conditions, the trans-synaptic labelling of neurons with rabies virus is retrograde and therefore useful for analysing premotor circuits.

Distinct motor circuits driven from wS1 and wM1

The subcortical axonal projections from wS1 and wM1 follow largely parallel pathways innervating neighbouring and largely non-overlapping brain areas (Matyas *et al.*, 2010). In the brainstem we found very little overlap in the regions innervated by wS1 and wM1 (Fig. 5). Projections from wS1 almost exclusively innervated the spinal trigeminal nuclei, including a ventral portion of Sp5O, lateral aspects of both rostral and caudal Sp5I and medial Sp5C. In contrast, wM1 primarily innervated PCRt, IRt, GIRt, MdV and MdD, while largely avoiding the spinal trigeminal nuclei. These distinct patterns of cortical innervation from wS1 and wM1 are likely to differentially activate the whisker premotor neurons in the brainstem.

To try to define the possible downstream motor circuits activated by cortical stimulation, we examined the overlap in the axonal projections from cortex with the locations of whisker premotor neurons. Because wS1 axons specifically innervate the spinal trigeminal nuclei (Fig. 5) and the majority of premotor neurons located in the spinal trigeminal nuclei are from the extrinsic muscle (Figs 3 and 4), we further investigated possible interactions finding close apposition of wS1 axon with extrinsic premotor neurons (Fig. 6). This raises the possibility that wS1 drives whisker retraction through a simple circuit wS1→Sp5Ir (extrinsic premotor)→FN (extrinsic motor; Fig. 6D). In future experiments it will be important to specifically inactivate the neurons in this proposed circuit to test this hypothesis.

Motor circuits in the brainstem downstream of wM1 appear more complex. In part, whisker movements evoked by wM1 might be driven by direct monosynaptic input onto motor neurons in the FN

(Grinevich *et al.*, 2005). Indeed, we found axons from wM1 inner-vating ventrolateral FN, where intrinsic motor neurons are located, and we also found monosynaptically connected premotor neurons in motor and frontal cortex from rabies injections into the intrinsic muscle. However, latencies for whisker movement evoked by wM1 stimulation were not shorter than the latencies for whisker move-ment evoked by wS1 stimulation. The direct monosynaptic innerva-tion of FN motor neurons by wM1 may therefore not be the most important circuit by which wM1 drives whisker movement. The densest axonal innervation from wM1 was found in PCRt, IRt, GIRt, MdV and MdD, which contain premotor neurons for both intrinsic and extrinsic muscles. The IRt, especially the region medial and dorsal to NA, contains a very high density of intrinsic premotor neurons (Figs 3D and 4C) and is strongly innervated by wM1 (Figs 5 and 7). Rhythmic whisker protraction driven by stimulation of wM1 might therefore be driven by a circuit wM1→IRt (intrinsic premotor)→FN (intrinsic motor) (Fig. 7F). Specific inactivation of the neurons in this proposed circuit will be critical to test this hypothesis in future experiments.

The movements evoked by wM1 stimulation are also more complex than those evoked by wS1. wM1 drives not only protraction but also rhythmic whisking (involving both protraction and retraction), whereas wS1 stimulation drives a constant whisker retraction. The greater complexity of the whisker movements evoked by wM1 stimu-lation may result from activation of more complex central pattern gen-erator circuits in the brainstem, which might also interact with the controllers of other orofacial movements (Moore *et al.*, 2013).

Functional implications and future perspectives

The whisker movements evoked by wS1 and wM1 are qualita-tively different and probably serve distinct functional roles during behaviour. The whisker retraction driven by wS1 might serve as a useful negative feedback signal, reducing the flow of incoming sensory information. The rhythmic whisker protraction evoked by wM1 stimulation resembles exploratory whisking and is thus probably involved in enhancing the flow of incoming information. These two different cortical regions thus evoke whisker move-ments with opposing purposes, probably through distinct motor circuits explored in this study. It is unknown whether similar antagonistic cortical motor circuits exist in other systems and species.

Motor control by sensory cortex is unusual (Matyas *et al.*, 2010) and it is possible that it is a unique specialization of the whisker system. The intrinsic muscles that drive whisking are also unusual in having no spindles for proprioception, and the motor control by wS1 might then provide valuable sensory input to the whisker motor system. On the other hand, motor control by sensory cortex might be of general importance, e.g. premotor neurons have been reported to be found in the macaque primary somatosensory cortex (Rathelot & Strick, 2006). In future experiments it will therefore be important to re-examine cortical motor maps and the possible downstream motor circuits in different species and systems.

Conflict of interests

The authors have no conflict of interests.

Acknowledgements

Abbreviations

ChR2, channelrhodopsin-2; FN, facial nucleus; GIRt, gigantocellular reticu-lar formation; HSV1-G, Herpes Simplex Virus 1-Glycoprotein; IRt, interme-diate reticular formation; LPG, lateral para-gigantocellular reticular formation; MdD, medullary dorsal reticular formation; MdV, medullary ven-tral reticular formation; NA, nucleus ambiguus; P, postnatal day; PCRt, par-vocellular reticular formation; PFA, paraformaldehyde; PSD, power spectral density; Rt, reticular formation; Sp5C, spinal trigeminal nucleus caudalis; Sp5Ic, spinal trigeminal nucleus caudal interpolaris; Sp5Ir, spinal trigeminal nucleus rostral interpolaris; Sp5O, spinal trigeminal nucleus oralis; Ve, ves-tibular nuclei; wM1, whisker motor cortex; wS1, whisker somatosensory cortex.

References

Berg, R.W. & Kleinfeld, D. (2003) Rhythmic whisking by rat: retraction as well as protraction of the vibrissa is under active muscular control. *J. Neu-rophysiol.*, **89**, 104–117.

Bosman, L.W., Houweling, A.R., Owens, C.B., Tanke, N., Shevchouk, O.T., Rahmati, N., Teunissen, W.H., Ju, C., Gong, W., Koekkoek, S.K. & De Zeeuw, C.I. (2011) Anatomical pathways involved in generating and sens-ing rhythmic whisker movements. *Front. Integr. Neurosci.*, **5**, 53.

Chan, C.H., Godinho, L.N., Thomaidou, D., Tan, S.S., Gulisano, M. & Par-navelas, J.G. (2001) Emx1 is a marker for pyramidal neurons of the cere-bral cortex. *Cereb. Cortex*, **11**, 1191–1198.

Crochet, S., Poulet, J.F.A., Kremer, Y. & Petersen, C.C.H. (2011) Synaptic mechanisms underlying sparse coding of active touch. *Neuron*, **69**, 1160–1175.

Curtis, J.C. & Kleinfeld, D. (2009) Phase-to-rate transformations encode touch in cortical neurons of a scanning sensorimotor system. *Nat. Neuro-sci.*, **12**, 492–501.

Diamond, M.E., von Heimendahl, M., Knutsen, P.M., Kleinfeld, D. & Ahis-sar, E. (2008) 'Where' and 'what' in the whisker sensorimotor system. *Nat. Rev. Neurosci.*, **9**, 601–612.

Dörfl, J. (1982) The musculature of the mystacial vibrissa of the white mouse. *J. Anat.*, **135**, 147–154.

Esposito, M.S., Capelli, P. & Arber, S. (2014) Brainstem nucleus MdV medi-ates skilled forelimb motor tasks. *Nature*, **508**, 351–356.

Graziano, M.S., Taylor, C.S. & Moore, T. (2002) Complex movements evoked by microstimulation of precentral cortex. *Neuron*, **34**, 841–851.

Grinevich, V., Brecht, M. & Osten, P. (2005) Monosynaptic pathway from rat vibrissa motor cortex to facial motor neurons revealed by lentivirus based axonal tracing. *J. Neurosci.*, **25**, 8250–8258.

Grinvald, A., Lieke, E., Frostig, R.D., Gilbert, C.D. & Wiesel, T.N. (1986) Functional architecture of cortex revealed by optical imaging of intrinsic signals. *Nature*, **324**, 361–364.

Haidarliu, S., Simony, E., Golomb, D. & Ahissar, E. (2010) Muscle architec-ture in the mystacial pad of the rat. *Anat. Rec.*, **293**, 1192–1206.

Haiss, F. & Schwarz, C. (2005) Spatial segregation of different modes of movement control in the whisker representation of rat primary motor cor-tex. *J. Neurosci.*, **25**, 1578–1587.

Harrison, T.C., Ayling, O.G. & Murphy, T.H. (2012) Distinct cortical circuit mechanisms for complex forelimb movements and motor map topography. *Neuron*, **74**, 397–409.

Hattox, A.M., Priest, C.M. & Keller, A. (2002) Functional circuitry involved in the regulation of whisker movements. *J. Comp. Neurol.*, **442**, 266–276.

Herfst, L.J. & Brecht, M. (2008) Whisker movements evoked by stimulation of single motor neurons in the facial nucleus of the rat. *J. Neurophysiol.*, **99**, 2821–2832.

Klein, B.G. & Rhoades, R.W. (1985) Representation of whisker follicle intrinsic musculature in the facial motor nucleus of the rat. *J. Comp. Neu-rol.*, **232**, 55–69.

Kleinfeld, D. & Deschênes, M. (2011) Neuronal basis for object location in the vibrissa scanning sensorimotor system. *Neuron*, **72**, 455–468.

Lein, E.S., Hawrylycz, M.J., Ao, N., Ayres, M., Bensinger, A., Bernard, A., Boe, A.F., Boguski, M.S., Brockway, K.S., Byrnes, E.J., Chen, L., Chen, L., Chen, T.M., Chin, M.C., Chong, J., Crook, B.E., Czaplinska, A., Dang,

C.N., Datta, S., Dee, N.R., Desaki, A.L., Desta, T., Diep, E., Dolbeare, T.A., Donelan, M.J., Dong, H.W., Dougherty, J.G., Duncan, B.J., Ebbert, A.J., Eichele, G., Estin, L.K., Faber, C., Facer, B.A., Fields, R., Fischer, S.R., Fliss, T.P., Frensley, C., Gates, S.N., Glattfelder, K.J., Halverson, K.R., Hart, M.R., Hohmann, J.G., Howell, M.P., Jeung, D.P., Johnson, R.A., Karr, P.T., Kawal, R., Kidney, J.M., Knapik, R.H., Kuan, C.L., Lake, J.H., Laramee, A.R., Larsen, K.D., Lau, C., Lemon, T.A., Liang, A.J., Liu, Y., Luong, L.T., Michaels, J., Morgan, J.J., Morgan, R.J., Mortrud, M.T., Mosqueda, N.F., Ng, L.L., Ng, R., Orta, G.J., Overly, C.C., Pak, T.H., Parry, S.E., Pathak, S.D., Pearson, O.C., Puchalski, R.B., Riley, Z.L., Rockett, H.R., Rowland, S.A., Royall, J.J. Ruiz, M.J., Sarno, N.R., Schaff-nit, K., Shapovalova, N.V., Sivisay, T., Slaughterbeck, C.R., Smith, S.C., Smith, K.A., Smith, B.I., Sodt, A.J., Stewart, N.N., Stumpf, K.R., Sunkin, S.M., Sutram, M., Tam, A., Teemer, C.D., Thaller, C., Thompson, C.L., Varnam, L.R., Visel, A., Whitlock, R.M., Wohnoutka, P.E., Wolkey, C.K., Wong, V.Y., Wood, M., Yaylaoglu, M.B., Young, R.C., Youngstrom, B.L., Yuan, X.F., Zhang, B., Zwingman, T.A. & Jones, A.R. (2007) Genome-wide atlas of gene expression in the adult mouse brain. *Nature*, **445**, 168–176.

Matyas, F., Sreenivasan, V., Marbach, F., Wacongne, C., Barsy, B., Mateo, C., Aronoff, R. & Petersen, C.C.H. (2010) Motor control by sensory cortex. *Science*, **330**, 1240–1243.

Mitchinson, B., Martin, C.J., Grant, R.A. & Prescott, T.J. (2007) Feedback control in active sensing: rat exploratory whisking is modulated by environmental contact. *P. Roy. Soc. B-Biol. Sci.*, **274**, 1035–1041.

Moore, J.D., Deschênes, M., Furuta, T., Huber, D., Smear, M.C., Demers, M. & Kleinfeld, D. (2013) Hierarchy of orofacial rhythms revealed through whisking and breathing. *Nature*, **497**, 205–210.

Paxinos, G. & Franklin, K. (2001) *The Mouse Brain in Stereotaxic Coordinates*, 2nd Edn. Academic Press, San Diego, CA.

Petersen, C.C.H. (2007) The functional organization of the barrel cortex. *Neuron*, **56**, 339–355.

Petersen, C.C.H. (2014) Cortical control of whisker movement. *Annu. Rev. Neurosci.*, **37**, 183–203.

Rathelot, J.A. & Strick, P.L. (2006) Muscle representation in the macaque motor cortex: an anatomical perspective. *Proc. Natl. Acad. Sci. USA*, **103**, 8257–8262.

Stepien, A.E., Tripodi, M. & Arber, S. (2010) Monosynaptic rabies virus reveals premotor network organization and synaptic specificity of cholinergic partition cells. *Neuron*, **68**, 456–472.

Takatoh, J., Nelson, A., Zhou, X., Bolton, M.M., Ehlers, M.D., Arenkiel, B.R., Mooney, R. & Wang, F. (2013) New modules are added to vibrissal premotor circuitry with the emergence of exploratory whisking. *Neuron*, **77**, 346–360.

Ugolini, G. (1995) Specificity of rabies virus as a transneuronal tracer of motor networks: transfer from hypoglossal motorneurons to connected second-order and higher order central nervous system cell-groups. *J. Comp. Neurol.*, **356**, 457–480.

Wickersham, I.R., Lyon, D.C., Barnard, R., Mori, T., Finke, S., Conzelmann, K., Young, J. & Callaway, E.M. (2007) Monosynptic restriction of transsynaptic tracing from single genetically targeted neurons. *Neuron*, **53**, 639–647.

Wickersham, I.R., Sullivan, H.A. & Seung, H.S. (2010) Production of glycoprotein-deleted rabies viruses for monosynaptic tracing and high-level gene expression in neurons. *Nat. Protoc.*, **5**, 595–606.

Yonehara, K., Balint, K., Noda, M., Nagel, G., Bamberg, E. & Roska, B. (2011) Spatially asymmetric reorganization of inhibition establishes a motion sensitive circuit. *Nature*, **469**, 407–410.

Zampieri, N., Jessell, T.M. & Murray, A.J. (2014) Mapping sensory circuits by anterograde transsynaptic transfer of recombinant rabies virus. *Neuron*, **81**, 766–778.